





PAPER • OPEN ACCESS

Single-step atmospheric pressure plasma jet deposition of copper

To cite this article: Francis Lockwood Estrin et al 2025 Flex. Print. Electron. 10 045004

View the article online for updates and enhancements.

You may also like

- Photonic-digital hybrid artificial intelligence hardware architectures: at the interface of the real and virtual worlds Lília M S Dias, Dinis O Abranches, Ana R Bastos et al.
- ICRH modelling of DTT in full power and reduced-field plasma scenarios using full wave codes

A Cardinali, C Castaldo, F Napoli et al.

- Global evidence that cold rocky landforms support icy springs in warming mountains Stefano Brighenti, Constance I Millar, Scott Hotaling et al.



Flexible and Printed Electronics



PAPER

OPEN ACCESS

Single-step atmospheric pressure plasma jet deposition of copper

RECEIVED

3 July 2025

REVISED

19 September 2025

ACCEPTED FOR PUBLICATION

2 October 2025

PUBLISHED

22 October 2025

Original content from this work may be used under the terms of the Creative Commons

Attribution 4.0 licence.

Any further distribution of this work must maintain attribution to the author(s) and the title of the work, journal citation and DOI.



Francis Lockwood Estrin 📵, Oliver S J Hagger 📵, Michael A Parkes and Daren J Caruana* 👨

Christopher Ingold Laboratories, Department of Chemistry, University College London, 20 Gordon St., London WC1 H0AJ, United Kingdom

* Author to whom any correspondence should be addressed.

E-mail: d.j.caruana@ucl.ac.uk

Keywords: plasma jet, metal printing, single step, copper deposition

Supplementary material for this article is available online

Abstract

Additive manufacturing's transformative potential in electronics hinges on the ability to precisely deposit copper onto diverse surfaces. Atmospheric pressure plasma jet deposition is a new approach, which allows the deposit of metallic copper onto a variety of surface using aqueous metal salt solutions-based precursors as ink. In this study, we compare the conductivity of copper tracks deposited using selection of copper salts. From detailed profiles and resistance measurements, the copper tracks from the chloride salt precursor, showed the highest conductivity, of $22\% \pm 7\%$ of bulk. Tracks formed using copper nitrate salt, showed only 1%-5% of bulk conductivity, suggesting that the anion, despite having no obvious chemical role in the deposition process has a significant effect on the resulting metal print quality. Characterisation using XRD, XPS, SEM and Raman, showed that all salts used as precursors produced fully reduced copper metal tracks by the plasma at 12 W. However, SEM revealed that both copper chloride and copper sulphate precursors lead to a high-density tracks, whereas copper salts of nitrate, acetate and formate lead to low density tracks. Furthermore, SEMs taken at short deposition times show the mechanism for the track deposition may explain the reason for the differences in conductivity.

1. Introductions

The printed electronics market is currently experiencing significant growth, driven by the demand for lightweight, flexible, and cost-effective electronic devices [1]. Deposition of highly conducting metallic interconnects is key for fulfilling this growing appetite for most electronic devices such as batteries, medical devices and photovoltaics. However, current methods rely on complex multi-step processes, involving complex inks and deposited on high temperature compatible substrates such as petroleum-based plastics. Furthermore, constraints run counter to the demands on the final metal print for integrity and function, for example flexible substrates for wearable technologies [2]. The need for a low cost, rapid and sustainable additive metal printing has never been greater [2–4].

Most flexible and circuit printing techniques use particle based inks deposited either using screen printing or ink/aerosol jet printers, directly depositing tracks in ink which are then cured to dry and sinter the nano-particles into a solid

contiguous track [5–7]. This curing step is performed using either high temperatures, UV-lights or corrosive chemicals, limiting the range of substrates that can be used and therefore the usability of these techniques [3]. Additionally the fabrication of the nano-particle inks can be expensive [8], limited shelf life and curing step can be slow [9].

More recent developments of metal deposition focus on the curing step either laser [10–14] or plasma [15–17]. These techniques still use a two-step deposition and curing, so remain slow, and often result in low adherence to the substrate. Sener et~al~ was able to demonstrate surface reduction of metal oxides to zero-valent metals in a single step [18] by exposure to an atmospheric pressure plasma jet (APPJ) opening the door to the development of single step deposition and reduction without the need for nanoparticle inks. With in-situ reduction for deposition from copper oxide also demonstrated, by Dey et~al~ [19], although they measured a high resistance (7 Ω) in the resulting copper sheets.

APPJs are formed by flowing an inert gas through a high voltage electric field. If this field is sufficiently strong the gas becomes ionized and forms a plasma. This plasma is expelled from an orifice, creating a plasma a jet discharge at atmospheric pressure [20-22]. Low power APPJ discharges can be cold enough to use on organic tissue [23] but are highly reactive [24]. APPJs have been used to cure deposited ink and to remove the organic components such as [15, 25]. However, recent work has shown that the plasma can also act as a reducing agent possibly by the action of the free electrons form the plasma gas [19, 26]. This one step process uses metal salts in aqueous solutions, directly aerosolised into the plasma gas, reduced to zero-valent metal and then deposited on the substrate [27-30]. Whilst the process appears to be quite generally applied to many metals, the role of the anion in solution as it passes through the plasma is not clear. Lockwood Estrin et al [30], did a direct sideby-side comparison for silver and copper nitrate salts, and showed that the silver showed significantly higher conductivities than for copper tracks under identical deposition conductions.

The majority of printed tracks are silver derivatives, making a technique capable of depositing copper interconnectors highly appealing. This is because copper has both economic and material advantages over silver. Copper is significantly cheaper and more readily available than silver, thus lowering total material costs, making circuit board printing more accessible [31]. Also, for complete circuit fabrication it is necessary to solder components to these tracks. Silver is unsuited for this purpose, as it is soluble in many solder solutions, unlike copper [31].

In this study the role of the anion in the plasma reduction and/or deposition process was investigated. Our starting postulate was that anions are there as spectator ions, having no major function but to maintain electroneutrality if or when required. We choose copper salts with a variety of different anions, such as nitrate, sulphate and chloride as well as organic anions such as formate and acetate to test this hypothesis. Copper metal was deposited in a side-by-side comparison under identical conditions. We report the conductivity of the resulting track as well as XPS and XRD.

2. Method

All the metal printing was been done with an inhouse designed and built plasma jet, described in detail in [30]. In brief, the plasma was driven by a 13.6 MHz impedance matched RF signal applied to the needle shown in figure 1. The RF signal was pulsed with variable duty cycle such that the ontime power is always 15 W, but the average power is variable to 6 W, 9 W and 12 W. All powers sustained a stable plasma extending 5–7 mm from the top of the nozzle, as shown in figure 1. The metal

was printed on borosilicate glass substrates with the ceramic nozzle of the jet positioned 1.5 mm above the glass. The glass substrate was placed on a grounded aluminium platform attached to an x-y-z motorised platform. During normal operation the plate is moved 10 mm transversally then returned to origin time at 1 mm s⁻¹, this process is repeated leaving an average deposition rate of 0.05 mm s⁻¹. The delivery rate of the salt into the plasma jet was $8.6 \pm 1.4 \times 10^{-10}$ moles s⁻¹.

All solutions were made by dissolving copper salts of nitrate (Cu(NO₃)₂), formate (Cu(CHOO)₂), acetate (Cu(C₂H₃O₂)₂), chloride (CuCl₂)and sulphate (CuSO₄) (Aldrich Chemical Company, >98% purity) in deionized water (18 M Ω m, ELGA) at a concentration of 5 mM. The solution containing the desired salt was injected into a Teledyne CETAC Technologies nebuliser at a rate of 0.5 ml min^{-1} . The fluid Injection rate was managed by a calibrated Harvard Apparatus syringe pump. The aerosol generated by the nebuliser was carried by the plasma gases comprising of helium (99.9+%, BOC) at 500 ml min^{-1} then later mixed with 25 ml min⁻¹ of hydrogen (99.9+%, BOC) a protective sheath gas of nitrogen flowed at rate of 2 l min⁻¹ to isolate the plasma from the atmosphere.

The deposited tracks were investigated using 3D optical imaging, Raman, XRD, XPS, four-point conductivity measurements and SEM imaging. Optical images were taken using a VHX-7000 optical microscope (Keyence Corporation), this microscope is capable of taking 3D optical images and is used for profilometry from which the cross section of the deposited tracks was determined. Raman spectroscopy was recorded using a Renishaw (inVia) confocal Raman microscope with an argon-ion laser excitation source (514.5 nm copper ion laser), between 100 cm^{−1} and 3200 cm^{−1}. XPS measurements were carried out using the ThermoFisher K-Alpha XPS supported by Advantage software. Analysis of data was carried out using CasaXPS software. The XRD system was a Bruker Vantec 500 k-Alpha run at 0.01° per step. Conductivity was performed using the Ossila four-point probe to measure both conductivity and sheet resistance for an assumed geometry of rectangular shape width 1 mm and 1 μ m thickness, modified by the measured width, thickness and cross sectional area. SEM was performed to inspect morphology of the sample using the JEOL 7600 SEM.

3. Results

It has been previously shown that copper and silver nitrate salts added to a hydrogen doped plasma jet in the form of an aerosol, may be reduced to zero-valent metal [30]. The metal reduction may be driven by the plasma electrons, but the reduction process is accelerated by the presence of hydrogen. The fate of the anion is not normally of much interest, as it is compositions

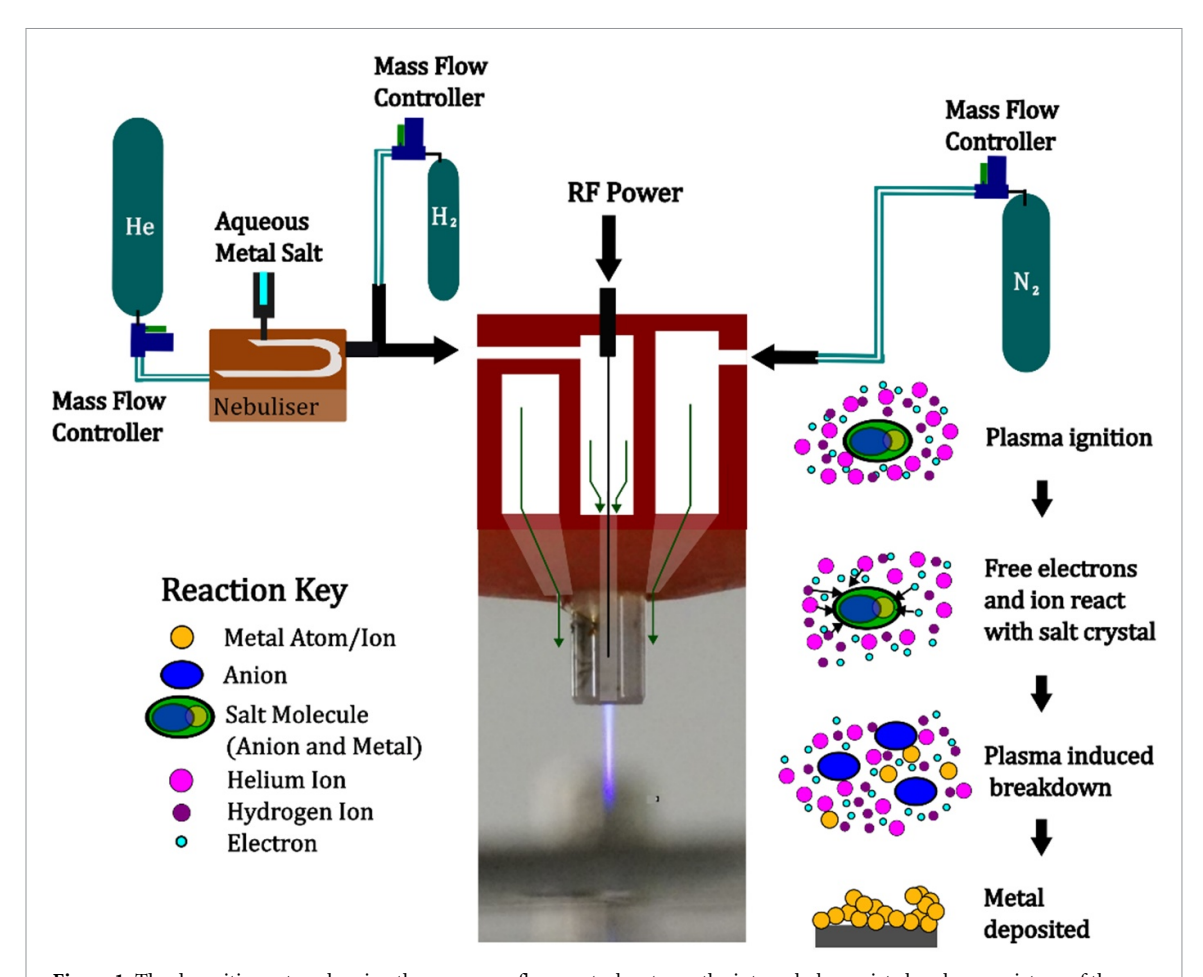


Figure 1. The deposition setup showing the power gas flow control systems, the internal plasma jet chambers, a picture of the ignited plasma and a diagram of the plasma induced salt breakdown. Gas flow through the plasma chamber is indicated by the dark green arrows.

not expected to directly participate in the reduction of the metal salt. To investigate the role of the anion, we used a variety of different copper salts to deposit metal tracks on glass substrates under identical conditions. Images of metal tracks using copper sulphate, chloride, acetate, formate and nitrate under 6 W, 9 W and 12 W power are shown in figure 2(a). From the optical images it can be clearly seen that, at 12 W power, all tracks are composed of zero-valent copper. Whereas when the power is reduced to 6 W there is no longer a distinct and clear orange colour indicating a lack of reduced copper. Copper salts are highly coloured when hydrated; sulphate and chloride salts appear white when dehydrated and anhydrous copper nitrate is green. Whereas reduced zero-valent copper has the distinct orange colour, the shade of this colour can be affected but the microstructure giving a difference in light reflection. Finally, copper oxide is black or red depending on oxidation state of the metal. The 6 W copper sulphate and copper chloride tracks are white indicating dehydrated unreduced copper salt. To confirm the oxidation state of the copper, XPS were recorded for the copper deposited using copper nitrate as the precursor at 6 W, 9 W and 12 W, shown in figure 2(b). At high power during the deposition, the peak at 935 eV reduces in intensity at higher powers and the peak at 932.5 eV becomes dominant. The peak at 932.5 eV is indicative of Cu 2p zero-valent metal, indicating that at higher power (>9 W) reduction is more effective. At 6 W, the reduction is incomplete with a significant proportion of copper that is in the Cu²⁺ state around 394.5 eV. Meaning the sample contains a significant percentage of Cu(NO₃)₂, Cu(OH)₂ or copper oxide. It should be noted that XPS is a surface technique and a small layer of surface oxidation is seen even at 12 W power. We have previously reported similar results in more detail but only using copper nitrate [30]. Raman spectroscopy, shows no measurable oxide or salt peaks (see supplementary material figure S1) from films deposited at 12 W, figure 2(c). Anion peaks are clear for the deposit at 6 W (supplementary material, figure S2). It should be noted that neither the zero-valent copper or some anion salts are Raman active. For this reason additional film investigation is needed before plasma reduction to zero-valent copper is confirmed. XRD spectrum of tracks deposited from every salt at all three powers is shown in figure 3. At 12 W all salts of copper tested form crystalline copper deposits. It can be seen that as the power is decreased the

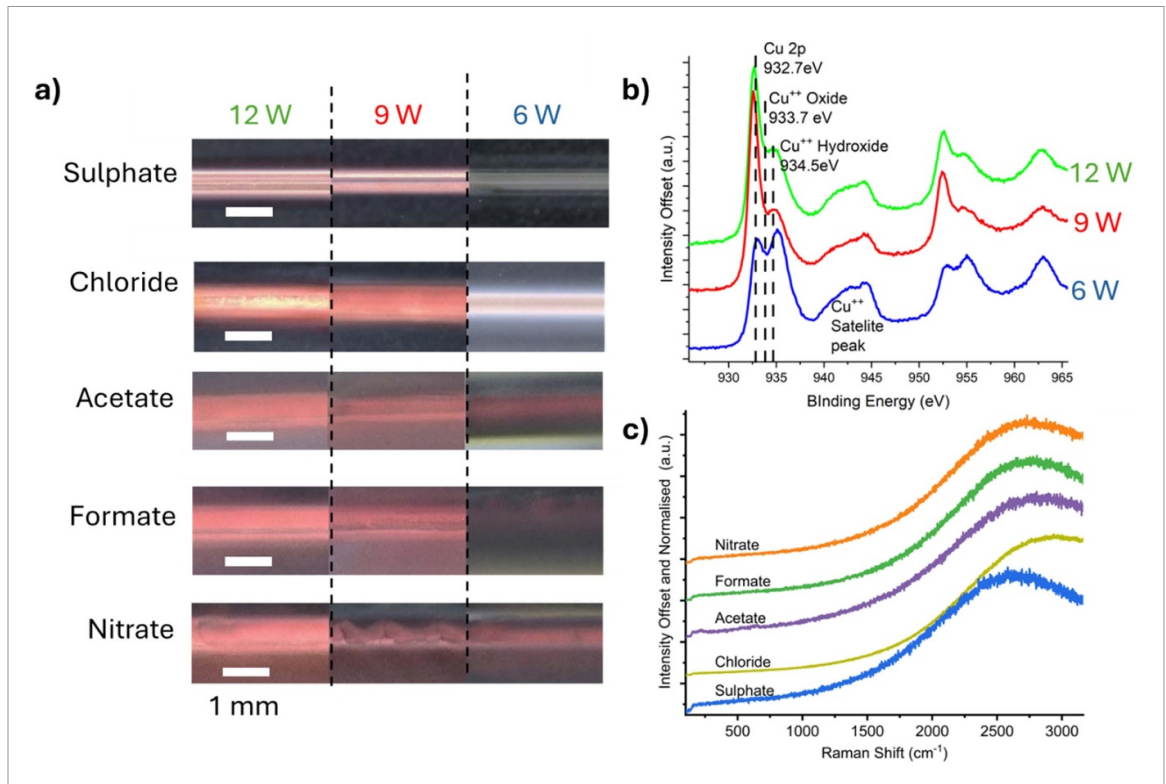


Figure 2. (a) Optical images of tracks deposited at 12 W, 9 W and 6 W from all salt solutions. (b) XPS of copper tracks deposited at 12 W, 9 W and 6 W for nitrate at the Cu 2p and Cu 2p1/2 peaks. (c) Raman spectra of tracks deposited at 12 W from all salt solutions, normalised and offset so each can be seen clearly.

XRD response decreases to almost not detectable at 6 W, with only minor peaks at (111) seen in nitrate, acetate and formate precursors. This matches what is seen in the images in figure 2(a). The drop in XRD signal indicates that at lower powers the plasma is unable to completely reduce copper salt to crystalline zero-valent metal. Whether this is because the copper becomes oxidised, fails to adhere to the surface, or left as unreduced salt, is unclear. The colour change, XPS and Raman, seen in figure 2(a), indicate a combination of all three at low plasma powers. Because, our primary concern is conductivity, the specific reasons for low level crystallinity was of second order concern, as the ultimate result for all is the highest conductive tracks. Further analysis of the (111) and (200) peak, in figures 3(c) and (d) reveals that the crystals making up the tracks have a slightly compressed lattice compared to the reference sample. The broad peaks shown in figure 3(c) indicate the sample is made up of a wide range of small crystals rather than a large single crystal structure. This indicator matches what has previously been observed [30]. However, for the most part these differences between samples are small. These results taken together show that the anion does not significantly change the power required to reduce the salt in the same way as the metal.

The conductivity of the zero-valent copper tracks vary significantly depending on the copper salt nebulised into the plasma jet; to understand this

variation the profile of the tracks deposited at 12 W is measured and shown in figure 4(c). This profile is used to calculate conductivity from the measured sheet resistance. Tracks produced using copper nitrate, acetates and formate solutions, all show similar low conductivity compared to bulk copper, while chloride and sulphate solutions have improved conductivity. Unremarkable sheet resistance, but vastly improved conductivity as shown for the copper tracks deposited using sulphate solutions is as a result of its smaller profiles, figure 4(c). Tracks produced using chloride solutions have around a quarter of bulk metal conductivity, whereas sulphate presents around 10% of bulk copper conductivity. The acetate's lower sheet resistance is canceled out by the thickness of the track, again due to the profile. Conductivity results from figure 4 are summarised in table 1. The sheet resistance as a function of print speed is shown in figure 4(d). Tracks deposited using chloride solutions perform well even when the print speed is increased, maintaining a sheet resistance of around 0.1 Ω \square^{-1} up to a speed of 0.2 mm s⁻¹, and then increases slightly, figure 4(d). The sheet resistance of silver nitrate is shown for comparison. The copper chloride compares favourably, but is still slightly worse in terms of performance.

The surface microstructure of the copper deposits from each of the salt solutions was examined by SEM. Images shown in figure 5, can, to a significant degree,

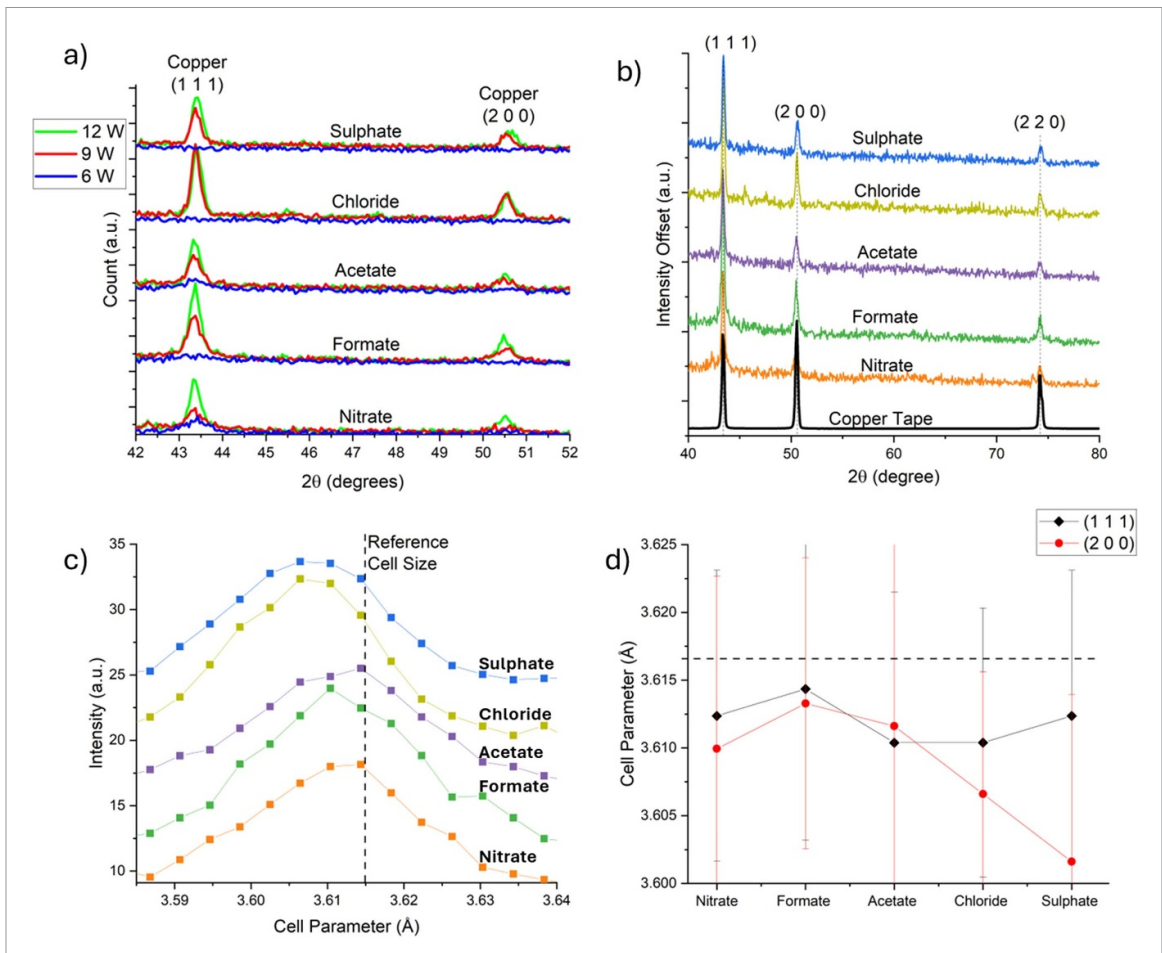


Figure 3. (a) the XRD of all tracks deposited from all five salt solutions inks at 12 W, 9 W and 6 W between 42° and 52° , with the (1 1 1) and (2 0 0) orientation peaks labelled. (b) XRD of the track deposited using all five salt solutions at 12 W power from a 5 mM solution, 1 mm s⁻¹ tracks with 20 times repetition compared against a copper sample 2θ between 40° and 80° with the orientations highlighted. (c) The cell parameter for each deposition calculated for the (1 1 1) peak and the calculated cell parameter for (1 1 1) and (2 0 0) peaks reference cell size of 3.6149 Å from Straumanis and Yu [32]. (d) The cell parameter change for (111) and (200) of the copper deposited from different salt solutions.

account for the reasons for the difference in the measured conductivity presented in figure 4(b). The tracks formed using copper nitrate, formate and acetate salt solutions all show a similar morphology; sintered sub 1 μ m metal particles with a reasonably open structure. On the other hand, copper tracks formed using sulphate and chloride solutions form a more compact and denser structure, with the sulphate salt having a more sintered and dense structure. The open structure shown for the nitrate, formate and acetate copper salt solutions leads to more dead space increasing cross-sectional area of the tracks accounting for the increase the sheet resistance observed. Whereas the copper tracks formed using sulphate and chloride solutions exhibit higher conductivities (lower sheet resistance) due to the condensed structure.

Deposited from copper chloride solutions seems to show gaps between the nano-particles. However, further inspection of the chloride track in supplementary information (figure S3) revealed that there are multiple layers beneath the ones visible in the figure 5. The 'sulphate' tracks are also tightly sintered,

however as shown by the profilometry in figure 4(c), they were extremely thin.

To gain deeper insight into the deposition process, a rapid deposition was carried out at 1 mm s⁻¹ to observe the early stages of track formation. Figure 6 shows SEM images at various magnifications for tracks formed using copper chloride, nitrate, and sulphate at an early stage of deposition. Several key observations may be made: (1) the rate of copper deposition from copper sulphate solutions was higher than that from both nitrate and chloride solutions; (2) copper deposition using nitrate and chloride salts produced a comparable particulate structure, at higher magnification, the extent of sintering appeared greater in the chloride samples; and (3) copper sulphate deposition resulted in smaller particles that only later coalesce into a continuous film. These observations somewhat align with the track profiles shown in figure 4(c). The low profile seen with sulphate is likely due to in-plane growth, forming a dense track with low sheet resistance, as presented in table 1. The difference in sintering between nitrate and chloride

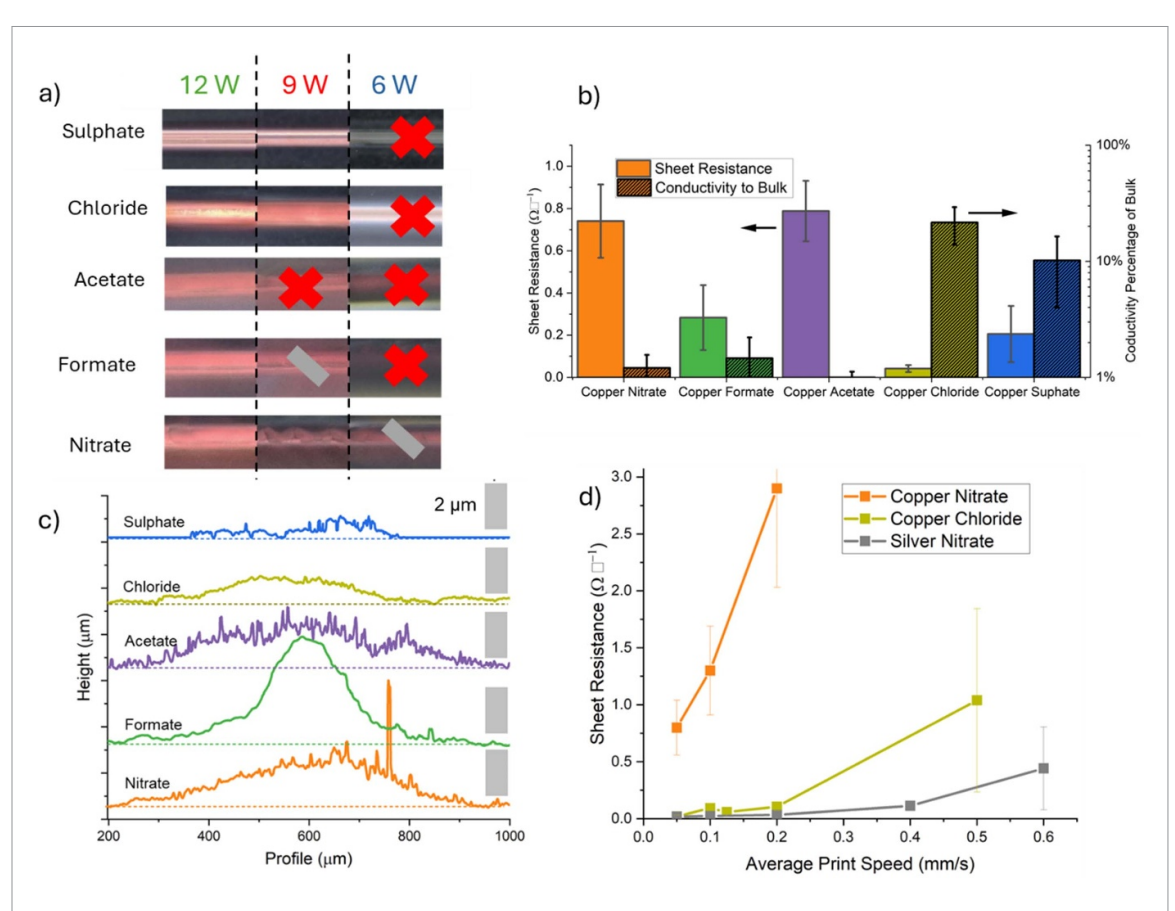


Figure 4. (a) Optical images with of track deposited from every salt where the no conductive tracks are marked with a red X and those where there has been a significant drop marked with w diagonal grey slash. With (b) the measured sheet resistance for the tracks deposited at 12 W and the conductivity as a percentage of bulk calculated from the cross sectional area found from (c) the profile of the copper tracks deposited at 12 W for all anions with a 2 μ m bar to indicate height. (d) The deposit speed against measured sheet resistance for copper nitrate and silver nitrate inks (previously measured in [30]) compared to copper chloride ink.

Table 1. The sheet resistance an conductivity in $MS m^{-1}$ and as a percentage of bulk for all anion inks.

Ink	Sheet resistance $(\Omega \square^{-1})$	Conductivity (MS m ⁻¹)	Percentage of bulk
Nitrate Formate Acetate Chloride Sulphate	$\begin{array}{c} 0.74 \pm 0.17 \\ 0.28 \pm 0.15 \\ 0.79 \pm 0.14 \\ 0.042 \pm 0.016 \\ 0.20 \pm 0.13 \end{array}$	$0.7 \pm .2$ $0.9 \pm .4$ $.58 \pm .09$ 13 ± 5 6 ± 4	$1.2 \pm .4$ $1.5 \pm .7$ $0.9 \pm .1$ 22 ± 7 7 ± 6

salts may also explain the lower profile and higher conductivity of chloride-based tracks compared to those formed with nitrate. However, early-stage morphological differences alone cannot fully account for the large discrepancy in conductivity, as nitrate and chloride demonstrate similar growth patterns but significantly different resistances.

4. Discussion

When copper chloride was used, the resulting tracks exhibited conductivity up to near 25% of bulk copper. Copper can now achieve similar conductivities to silver [30], although doing so requires higher powers,

regardless of the anion present in the copper salt. SEM images in figures 5 and 6 show that, when the chloride and sulphate salts are used, both the conductivity and track morphology closely resemble those of highly conducting silver-based tracks as reported in [30] and shown in the supplementary material. In contrast, tracks formed using acetate, formate, and nitrate salts are significantly more diffuse and open, leading to a reduced conductivity. While tracks produced using copper sulphate were denser but too thin to function as effective conductors. These findings suggest that conductivity and power requirements are not strongly correlated, and that anion removal plays a far more critical role in copper deposition than previously assumed.

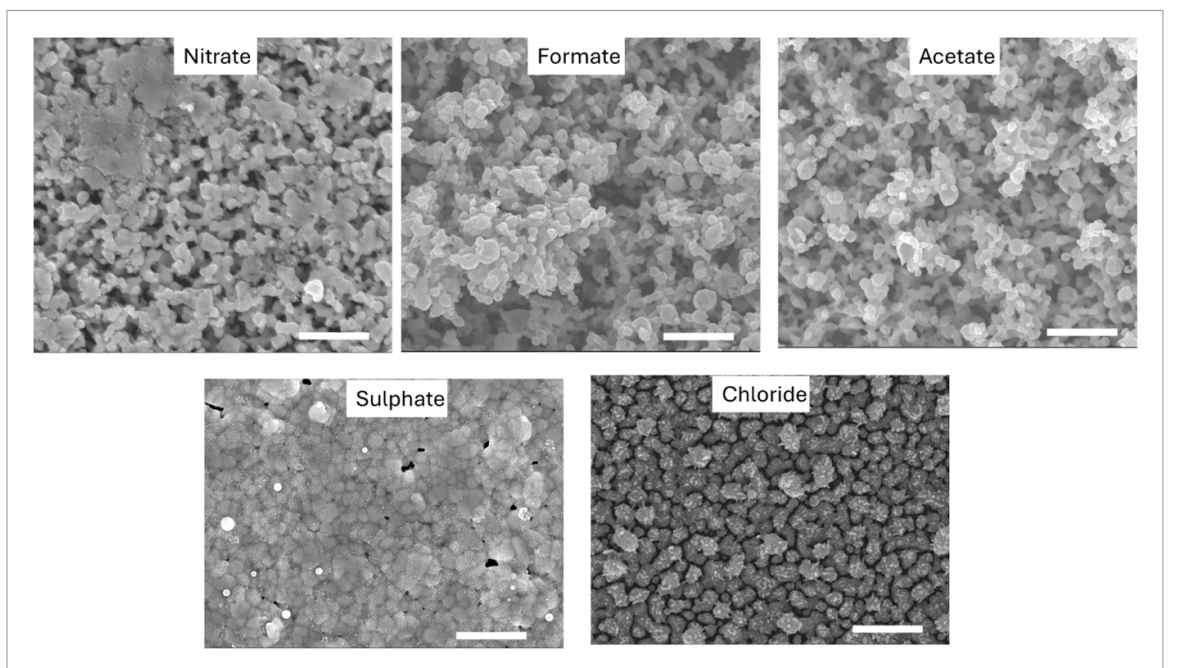


Figure 5. SEM images of the track deposited using all five anion solutions at 12 W power from a 5 mM solution, 1 mm/tracks with 20 times repartition, 1 mm/tracks with 20 times repetition with a 2 μ m bar.

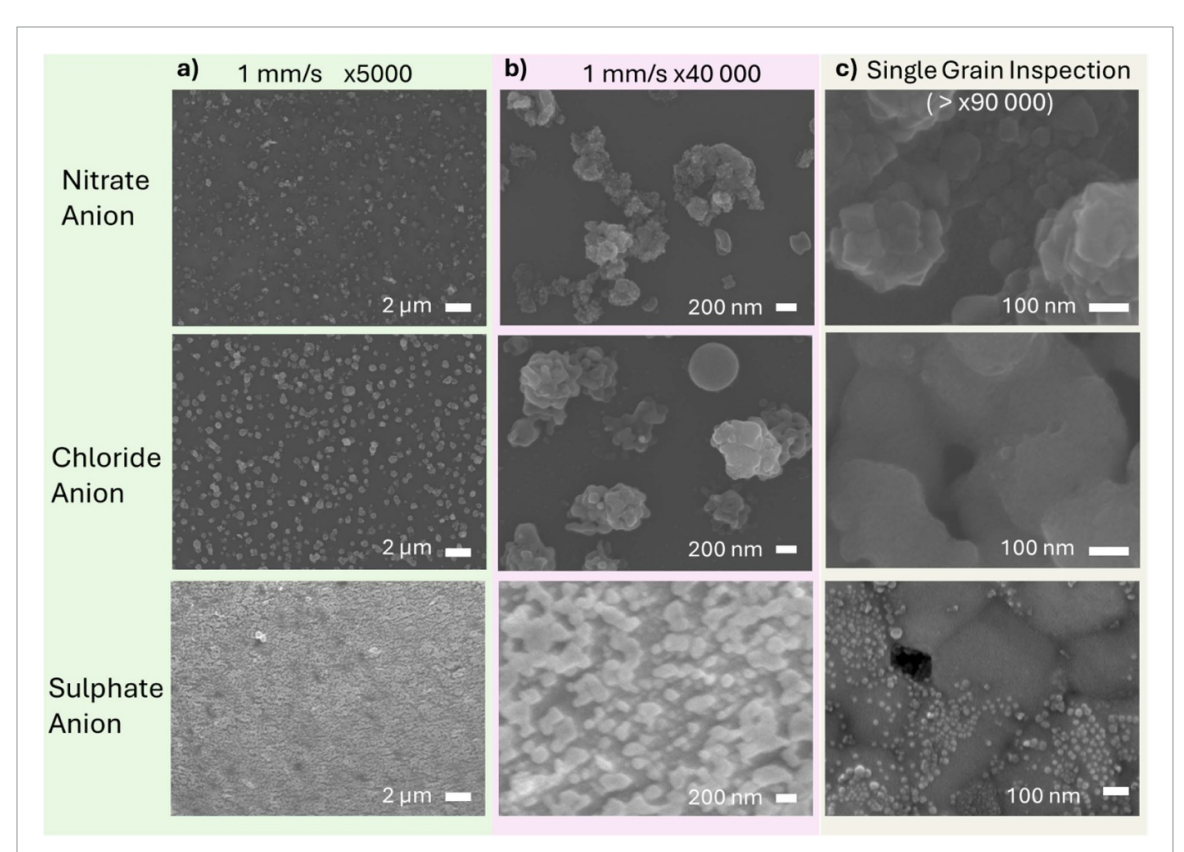


Figure 6. SEM images of the early stage of deposition, one pass 1 mm s $^{-1}$ of deposition for different anions (12 W power) for x5000 (a) and x40 000 (b) of nitrate, chloride and sulphate anions. With (c), an SEM image of x95 000 or greater zoom of a more complete deposition .showing how the track evolves at a smaller scale, x3 1 mm s $^{-1}$ nitrate (x150 000) and chloride(x150 000) and x20 1 mm s $^{-1}$ sulphate (x95 000) .

Further to this, SEM images presented in figure 6 provide valuable insights into how the metal deposits are formed and, more importantly, how they merge to create a conductive track. All copper tracks

appear to be composed of nano-particulates; however, higher-conductivity tracks appear to have efficiently coalesced and grow laterally, resulting in fewer gaps. Copper deposited from nitrate solutions lack this ability to fully coalesce and thus give a lower conductivity. As these particles grow, they shadow the base layer, preventing copper from filling the gaps and resulting in a porous, aerated substrate. Whereas the sulphate and chloride salts produce flatter and denser morphologies, showing significantly different structures even at early-stages.

Clearly, the anion has a very significant effect on morphology of the resulting track, as shown by the SEMs and conductivity but not a high influence on the extent of reduction of the metal. It is conceivable that the anion may be involved indirectly through the balance of charge during the reduction of the metal by either the plasma electrons or by hydrogen. The salt arrives to the plasma as a crystal after the aerosol is dehydrated by the nebuliser. The question raised by these results is the location of the copper reduction; i.e. either gaseous within the plasma or on the surface. If the electrons react with the salt crystal in the gas phase plasma, by reducing the metal salt to zerovalent metal, the crystal will gain a number of negative charges, which will charge the particle, and ultimately can inhibit further reduction through space charge effects. However, to a certain degree this charge may be neutralised by positive ions from the plasma. If the reduction occurs on the surface this charging may be dissipated to the surface and may not be an issue.

The reduction process is certainly dependent on the plasma, as the reduction does not take place with the carrier gases alone, i.e. hydrogen (4%) doped helium in absence of plasma. Reduction occurs only when the plasma is ignited. It is not possible with any great certainty, to state that the reduction is carried out solely by plasma electrons. However, we have shown fairly conclusively that plasma electrons do reduce metal oxides to zero-valent metal on surfaces in absence of hydrogen [18, 26]. It is likely that a mixed reduction by action of hydrogen species and plasma electrons is most probable. We can state that the anion may be removed by the hydrogen species within the plasma, concurrently with the reduction, to form the corresponding acid, e.g. HNO₃. Interestingly, we have not been able to detect any acid residue on or beside the deposited copper track. Nevertheless, it is highly likely that this is produced. Interestingly, the boiling point for the nitric acid, formic acid and acetic acid are fairly close together, 83, 100 and 117 °C, respectively. Although the precise temperature of the metal surface during deposition may be quite high, it is conceivable that nitric acid, acetic acid and formic acid may boil off and removed away from the deposition area. Whereas, the boiling point for HCl and H₂SO₄ are -85 and 337 °C. It is probably unlikely that the surface temperature reaches the boiling point of sulphuric acid, but still, no sulphate is found within or on the copper deposit using XPS or Raman. Even at ambient temperature HCl is a gas, meaning this can be readily lost from the metal deposition zone. Nevertheless, the extreme boiling points for the sulphuric and hydrochloric acids may be the reasons to the difference in the morphology observed for the copper metal deposited using CuSO₄ and CuCl₂ and the other salts.

The results presented in this work demonstrate that the measured resistance of plasma-deposited copper tracks is approaching, and in some cases has reached, values that render the technology potentially viable for use in electronic manufacturing. Nonetheless, further optimisation is required before industrial adoption can be realised, primarily in two key areas. Firstly the current track width presented in figure 4(c) is probably too wide to be viable for typical circuit interconnectors. This limitation could be addressed through refinement of the jet nozzle [30]. Secondly, for adoption as an integral industrial process, deposition time will have a critical influence on production cost. Therefore, for this process to become viable, print speed needs to be improved, an area we are currently focusing on. Beyond electrical conductivity, the broader advantages of plasma jet deposition are noteworthy. The deposited tracks exhibit high adherence on multiple surfaces and over conformal surfaces [28, 30]. Particle free inks, reduces material consumption, eliminates the need for noxious solvents or reactive chemicals. Although helium is required for plasma formation, it is not consumed during the process and may be recycled. Hydrogen currently at (4%) within the helium carrier gas is the only consumable. Together these factors highlight the considerable potential of atmospheric pressure plasma jet deposition for selected applications in electronic manufacture.

5. Conclusion

These results show that by changing the salt from copper nitrate to copper chloride, it is possible to produce tracks with a sheet resistance of 0.042 \pm 0.016 Ω \Box^{-1} and a conductivity of 13 \pm 7 MS m $^{-1}$ between 20%–25% of bulk copper conductivity. This significantly increases the viability of copper circuit interconnects produced via plasma deposition. Several anion-based inks were tested; however, none achieved the same level of conductivity or low resistance. That said, for applications where surface area coverage is more critical than conductivity, e.g. for barrier coatings, formate-based inks may be more suitable.

Data availability statement

All data that support the findings of this study are included within the article (and any supplementary files).

Acknowledgment

This work was supported by EPSRC Project Number EP/T024836/1. OSJH would like to acknowledge Dstl for an ICASE.

Conflict of interest

DJC holds a patent (Patent Application Number (PCT/EP2019/074106). No other conflict of interest.

Author contributions

Francis Lockwood Estrin © 0000-0002-1922-1124
Data curation (equal), Investigation (equal),
Methodology (equal), Writing – original
draft (equal)

Oliver S J Hagger 0 0000-0001-7336-8082 Data curation (equal), Methodology (equal)

Michael A Parkes

Data curation (equal), Formal analysis (equal), Project administration (equal), Writing – review & editing (equal)

Daren J Caruana © 0000-0002-8549-0621 Conceptualization (equal), Funding acquisition (equal), Project administration (equal), Supervision (equal), Writing – review & editing (equal)

References

- Buga C S and Viana J C 2022 The role of printed electronics and related technologies in the development of smart connected products Flex. Print. Electron. 7 043001
- [2] Maddipatla D, Narakathu B B and Atashbar M 2020 Recent progress in manufacturing techniques of printed and flexible sensors: a review *Biosensors* 10 199
- [3] Wu W 2017 Inorganic nanomaterials for printed electronics: a review *Nanoscale* 9 7342–72
- [4] Koo J H, Seo J and Lee T 2012 Nanomaterials on flexible substrates to explore innovative functions: from energy harvesting to bio-integrated electronics *Thin Solid Films* 524 1–19
- [5] Cummins G and Desmulliez M P Y 2012 Inkjet printing of conductive materials: a review Circuit World 38 193–213
- [6] Tao R, Peng J, Ning H, Chen J, Zou J, Fang Z, Yang C, Zhou Y, Zhang J and Yao R 2018 Inkjet printed electrodes in thin film transistors *IEEE J. Electron. Devices Soc.* 6 774–90
- [7] Zeng X, He P, Hu M, Zhao W, Chen H, Liu L, Sun J and Yang J 2022 Copper inks for printed electronics: a review Nanoscale 14 16003–32
- [8] Beedasy V and Smith P J 2020 Printed electronics as prepared by inkjet printing *Materials* 13 704
- [9] Halonen E, Viiru T, Ostman K, Cabezas A L and Mantysalo M 2013 Oven sintering process optimization for inkjet-printed Ag nanoparticle ink *IEEE Trans. Compon. Packag. Manuf. Technol.* 3 350–6
- [10] Zhou X, Guo W and Peng P 2021 Laser erasing and rewriting of flexible copper circuits Nano-Micro Lett. 13 184
- [11] Jones J, Snowdon M R, Rathod S and Peng P 2023 Direct laser writing of copper and copper oxide structures on

- plastic substrates for memristor devices Flex. Print. Electron. 8 015008
- [12] Zhou X, Guo W, Fu J, Zhu Y, Huang Y and Peng P 2019 Laser writing of Cu/CuO integrated structure on flexible substrate for humidity sensing Appl. Surf. Sci. 494 684–90
- [13] Renn M J, Schrandt M, Renn J and Feng J Q 2017 Localized laser sintering of metal nanoparticle inks printed with aerosol Jet® technology for flexible electronics J. Microelectron. Electron. Packag. 14 132–9
- [14] Zhao W, Rovere T, Weerawarne D, Osterhoudt G, Kang N, Joseph P, Luo J, Shim B, Poliks M and Zhong C-J 2015 Nanoalloy printed and pulse-laser sintered flexible sensor devices with enhanced stability and materials compatibility ACS Nano 9 6168–77
- [15] Gandhiraman R P, Singh E, Diaz-Cartagena D C, Nordlund D, Koehne J and Meyyappan M 2016 Plasma jet printing for flexible substrates Appl. Phys. Lett. 108 123103
- [16] Ramamurti R, Gandhiraman R P, Lopez A, Doshi P, Nordlund D, Kim B and Meyyappan M 2020 Atmospheric pressure plasma printing of nanomaterials for IoT applications IEEE Open J. Nanotechnol. 1 47–56
- [17] Öhlund T, Örtegren J, Forsberg S and Nilsson H-E 2012 Paper surfaces for metal nanoparticle inkjet printing Appl. Surf. Sci. 259 731–9
- [18] Sener M E, Sathasivam S, Palgrave R, Cabrera R Q and Caruana D J 2020 Patterning of metal oxide thin films using a H₂/He atmospheric pressure plasma jet *Green Chem*. 22 1406–13
- [19] Dey A, Lopez A, Filipič G, Jayan A, Nordlund D, Koehne J, Krishnamurthy S, Gandiraman R P and Meyyappan M 2019 Plasma jet based *in situ* reduction of copper oxide in direct write printing *J. Vac. Sci. Technol. B* 37 031203
- [20] Algwari Q T and O'Connell D 2011 Plasma jet interaction with a dielectric surface *IEEE Trans. Plasma Sci.* 39 2368–9
- [21] Ghimire B, Briggs E F, Sysoeva T A, Mayo J A and Xu K G 2023 Contrasting the characteristics of atmospheric pressure plasma jets operated with single and double dielectric material: physicochemical characteristics and application to bacterial killing J. Phys. D: Appl. Phys. 56 085205
- [22] Schutze A, Jeong J Y, Babayan S E, Park J, Selwyn G S and Hicks R F 1998 The atmospheric-pressure plasma jet: a review and comparison to other plasma sources *IEEE Trans. Plasma Sci.* 26 1685–94
- [23] Reuter S, von Woedtke T and Weltmann K-D 2018 The kINPen—a review on physics and chemistry of the atmospheric pressure plasma jet and its applications J. Phys.: Appl. Phys. 51 233001
- [24] Dias T C, Fromentin C, Alves L L, Tejero-del-caz A, Silva T and Guerra V 2023 A reaction mechanism for oxygen plasmas *Plasma Sources Sci. Technol.* 32 084003
- [25] Manzi J, Weltner A E, Varghese T, McKibben N, Busuladzic-Begic M, Estrada D and Subbaraman H 2023 Plasma-jet printing of colloidal thermoelectric Bi₂Te₃ nanoflakes for flexible energy harvesting *Nanoscale* 15 6596–606
- [26] Sener M E and Caruana D J 2018 Modulation of copper(I) oxide reduction/oxidation in atmospheric pressure plasma jet *Electrochem. Commun.* 95 38–42
- [27] Hagger O S J, Sener M E, Khan I, Estrin F L, Agrotis S, Handoko A D, Parkin I P and Caruana D J 2023 Rapid single step atmospheric pressure plasma jet deposition of a SERS active surface *Mater. Adv.* 4 3239–45
- [28] Hagger O S J, Parkes M A, Lockwood Estrin F, Agrotis S, Parkin I P, Handoko A D and Caruana D J 2025 Additive metal printing on multi materials using an atmospheric pressure plasma jet on a 5-Axis platform *Mater. Des.* 251 113681

- [29] Agrotis S, Sener M E, Hagger O S J, Handoko A D and Caruana D J 2024 One-Step synthesis of nanosized Cu-Ag films using atmospheric pressure plasma jet Appl. Mater. Today 39 102286
- [30] Lockwood Estrin F, Hagger O S J, Sener M E and Caruana D J 2024 Metal painting by plasma jet Adv. Mater. Interfaces 11 2400256
- [31] Li X, Andersson H, Sidén J and Schön T 2018 Soldering surface mount components on screenprinted Ag patterns on paper and polyimide substrates for hybrid printed electronics Flex. Print. Electron. 3 015003
- [32] Straumanis M E and Yu L S 1969 Lattice parameters, densities, expansion coefficients and perfection of structure of Cu and of Cu-In a phase Acta Cryst. A25 767